Polymer Journal (2023) 55:489–496
https://doi.org/10.1038/s41428-022-00726-9

ORIGINAL ARTICLE

Conjugated polymers with thiophene-fused thiaborin units and their strong intermolecular interactions

Yohei Adachi[1] · Mitsuru Sakabe[1] · Takanori Nomura[1] · Joji Ohshita[1,2]

Received: 27 July 2022 / Revised: 8 September 2022 / Accepted: 28 September 2022 / Published online: 16 November 2022
© The Society of Polymer Science, Japan 2022

Abstract

Boron-incorporated p−π* conjugated polymers have been studied as optoelectronic and sensor materials. p−π* conjugated polymers usually possess bulky aryl groups that kinetically stabilize the boron centers, and the bulky aryl substituents prohibit intermolecular interactions in the solid state, thereby limiting the application of the polymers to semiconductors. In this work, we synthesized a thiophene-fused thiaborin unit as a new building block. The thiaborin monomer was facilely converted into distannyl and diiodo derivatives via lithiation. The p−π* conjugated polymers with the thiaborin unit exhibited well-defined redshifts in the absorption spectra measured in the film state relative to those measured in solution, suggesting strong intermolecular interactions.

Introduction

The preparation of new conjugated polymers is essential for the development of optoelectronic materials because conjugated polymers have specific features, such as a low-energy band gap and semiconducting properties [1–4]. Among the π-conjugated systems, conjugated polymers containing tricoordinate boron in the main chain are called p−π* conjugated polymers [5–8]. The interaction of the boron p-orbital with the adjacent π*-orbital results in the low-lying LUMO energy levels of p−π* conjugated polymers. In addition, thanks to its high Lewis acidity, tricoordinate boron is able to associate with Lewis bases, which gives rise to changes in optical properties due to the disappearance of the p−π* interaction. Therefore, p−π* conjugated polymers have been widely applied as sensor materials for the detection of Lewis bases such as amines, fluoride, and cyanide [9–11]. Many p−π* conjugated polymers have been developed following the pioneering work of Chujo et al. [12, 13]. These polymers, however, have one drawback—bulky aryl substituents must be introduced on the boron atom. As less bulky triarylboranes gradually decompose because they are hydrolyzed in air, 2,4,6-trimethylphenyl (Mes), 2,4,6-triisopropylphenyl (Tip), 2,4,6-tri-*tert*-butylphenyl (Mes*), and 2,4,6-tris(trifluoromethyl)phenyl (^{F}Mes) groups are commonly introduced on boron to improve the chemical stability of p−π*-conjugated polymers [5–8]. For example, Jäkle's group reported that ^{F}Mes-substituted dithienylborane (**^{F}BDT**) is a useful building unit for p−π*-conjugated polymers (Fig. 1) [14–18]. The bulky ^{F}Mes group not only stabilizes the compound kinetically but also enhances the electron-deficient property by the introduction of fluorine atoms. The high chemical stability, the low-lying LUMO energy level, and the easy functionalization of the thiophene rings of ^{F}BDT have facilitated the use of ^{F}BDT-based p−π* conjugated systems as n-type semiconducting materials [19–22]. On the other hand, the bulky ^{F}Mes group prevents strong intermolecular interactions, which is unfavorable for the development of n-type semiconductors with high electron mobility. For example, we have previously reported conjugated copolymers composed of ^{F}BDT and dithienosilole, **p(^{F}BDT-DTS)** (Fig. 1). Although **p(^{F}BDT-DTS)** exhibited an extended conjugation via the boron p-orbital, the absorption spectrum measured in the solid state was no different from that

Supplementary information The online version contains supplementary material available at https://doi.org/10.1038/s41428-022-00726-9.

✉ Yohei Adachi
yadachi@hiroshima-u.ac.jp

✉ Joji Ohshita
jo@hiroshima-u.ac.jp

[1] Smart Innovation Program, Graduate School of Advanced Science and Engineering, Hiroshima University, Higashi-Hiroshima 739-8527, Japan

[2] Division of Materials Model-based Research, Digital Monozukuri (Manufacturing) Education and Research Center, Hiroshima University, Higashi-Hiroshima 739-0046, Japan

measured in solution, implying limited intermolecular interactions in the solid state [16].

One way to enhance the intermolecular interactions in ^{F}BDT-based p−π* conjugated systems is to fix the dihedral plane between the two thiophene rings. Similar to ^{F}BDT, Mitsudo and Suga reported nitrogen-bridged dithienylborane DTNB (Fig. 1) [23]. The six-membered azaborin structure was responsible for the high aromaticity in the central ring, which improved the chemical stability. The planar structure of DTNB enabled π–π stacking in the crystal structure. However, the high aromaticity of the azaborin ring inhibited the extension of conjugation with the neighboring π-systems via the thiophene rings so that even in systems with extended π-systems, the absorption was limited to the UV region. In 2017, Liu et al. reported sulfur-bridged dithienylborane **DTSB** (Fig. 1) [24]. The moderate aromaticity of the thiaborin ring not only stabilized the compound but also realized the extension of conjugation. The sulfur atom was also expected to enhance the intermolecular interactions by the fixed planarity of the two thiophene rings and the sulfur–sulfur interactions [25–28]. However, to the best of our knowledge, no details of the intermolecular interactions of dithienylboranes containing the thiaborine structure have been reported. In this work, we synthesized S-bridged ^{F}BDT, **^{F}DTSB**, and its copolymers with bithiophene units. The prepared polymers exhibited well-defined redshifts in the absorption spectra measured in the film state relative to those measured in solution, which were not observed in **p(^{F}BDT-DTS)** [16], proving the stronger intermolecular interactions of **p(^{F}DTSB-DTS)** and **p(^{F}DTSB-2T)** than **p(^{F}BDT-DTS)**.

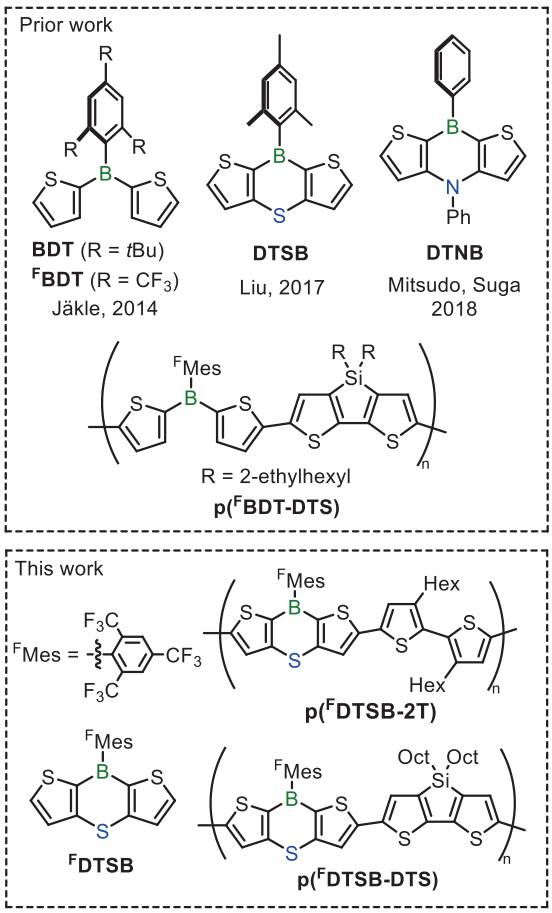

Fig. 1 Reported element-bridged and unbridged dithienylboranes

Results and discussion

Synthesis

The ^{F}Mes-substituted thiaborin unit **^{F}DTSB** was synthesized as shown in Scheme 1. Silicon-bridged precursor **2** was treated with BBr_3 to give a thiaborin intermediate with a bromine atom on the boron. The ^{F}Mes group was introduced by treating the intermediate with lithiated 1,3,5-tris(trifluoromethyl)benzene. **^{F}DTSB** was obtained as a white solid that is soluble in common organic solvents such as toluene, THF, and dichloromethane. **^{F}DTSB** did not decompose even after storage for one year in air at room temperature, reflecting its high chemical stability due to kinetic stabilization by the ^{F}Mes group and thermodynamic stabilization by the aromaticity of the thiaborin ring. The external α-protons of **^{F}DTSB** were easily deprotonated by *n*-butyllithium, and the subsequent treatment with tributyltin chloride or elemental iodine provided **^{F}DTSB-Sn** or **^{F}DTSB-I**, respectively (Scheme 1). **^{F}DTSB-Sn** was used

Scheme 1 Synthetic scheme of **^{F}DTSB** and its derivatives

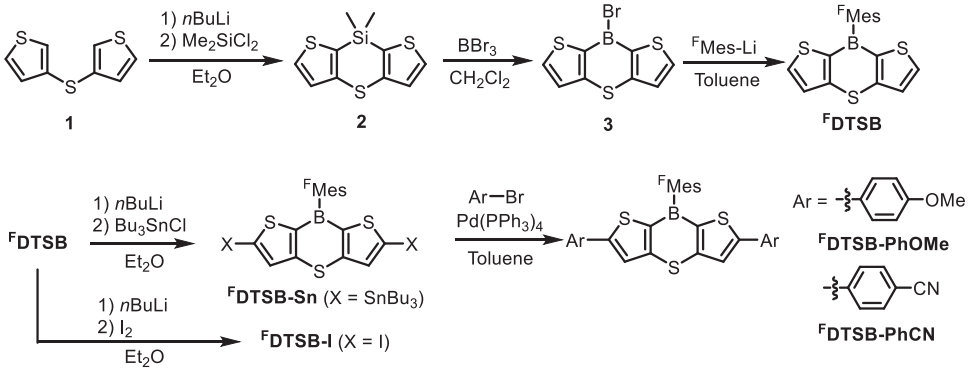

for palladium-catalyzed Stille cross-coupling reactions. To investigate the effect of the extension of the conjugation, two model compounds, **^{F}DTSB-PhOMe** and **^{F}DTSB-PhCN**, with an electron-donating methoxy group and an electron-deficient cyano group, respectively, were prepared by Stille cross-coupling reactions.

Single-crystal X-ray structure

Although various methods and solvents were employed, single crystals of **^{F}DTSB** could not be obtained. Fortunately, single crystals of **^{F}DTSB-PhOMe**, which have sufficient quality for single-crystal X-ray analysis, were obtained by slow evaporation from a dichloromethane/hexane solution. As shown in Fig. 2, the X-ray structure revealed the planar thiophene-fused thiaborin structure and the perpendicularly aligned ^{F}Mes group and was similar to the previously reported X-ray structure of **DTSB** [24]. The internal B – C bond lengths were much shorter than the external B – C(^{F}Mes) bond lengths. In addition, the C – S bond lengths in the thiaborin ring were nearly the same as the thiophene C – S bond lengths. These results clearly indicate the moderately high aromaticity of the thiaborin ring for thermodynamic stabilization. Indeed, the harmonic oscillator model of aromaticity (HOMA) [29, 30] value of the thiaborin ring was 0.63 for the X-ray structure (Table S1), confirming the moderately high aromaticity. The **^{F}DTSB-PhOMe** molecules were oriented in such a way that their long axis was parallel to the *c*-axis and avoided the steric hindrance of the bulky ^{F}Mes groups (Fig. S1). Contrary to our expectations, no strong intermolecular interactions, such as sulfur–sulfur and π–π interactions, were detected, and only weak CH – π interactions were observed in the crystal structure of **^{F}DTSB-PhOMe**.

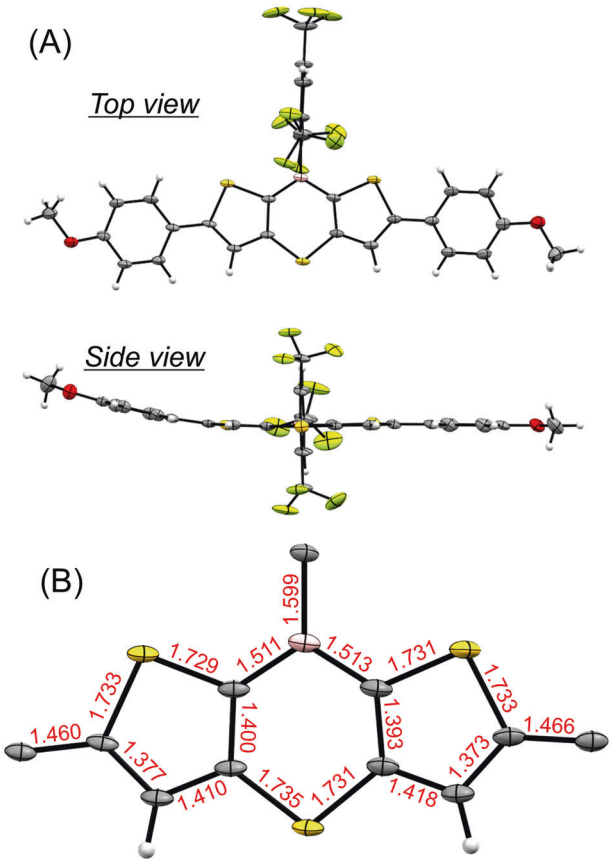

Fig. 2 Single-crystal X-ray structure (**A**) and bond lengths of the main structure (**B**) of **^{F}DTSB-PhOMe** obtained at 100 K. Thermal ellipsoids are at the 50% probability level

Optical properties

The UV-vis absorption and fluorescence spectra of **^{F}DTSB**, aryl-substituted **^{F}DTSB-PhCN**, and **^{F}DTSB-PhOMe** are shown in Fig. 3. The absorption maximum of **^{F}DTSB** was 350 nm in toluene and nearly the same as that of **DTSB** (347 nm in THF) [24], indicating the limited effect of the substituent on boron. The redshifted absorption spectra of phenyl-substituted **^{F}DTSB-PhCN** and **^{F}DTSB-PhOMe** relative to the **^{F}DTSB** absorption spectrum demonstrated that the conjugation was effectively extended via the boron p-orbital (Table 1). The absorption maximum of **^{F}DTSB-PhOMe** had a slightly longer wavelength than that of **^{F}DTSB-PhCN**, suggesting the presence of donor−acceptor (D – A) intramolecular interactions between the electron-deficient thiaborin unit and the electron-donating methoxyphenyl groups. No solvent dependence was observed in the absorption spectra of any of the compounds (Fig. S2, Table S2). Similar to the absorption, the fluorescence bands of **^{F}DTSB-PhCN** and **^{F}DTSB-PhOMe** were redshifted from that of nonsubstituted **^{F}DTSB** as a result of π-extension (Fig. 3). In contrast to the lack of solvent dependence of the fluorescence maxima of **^{F}DTSB-PhCN**, the fluorescence maxima of **^{F}DTSB-PhOMe** were gradually shifted to lower energies as solvent polarity was increased (Fig. S3, Table S2). This suggests that the fluorescence originates in

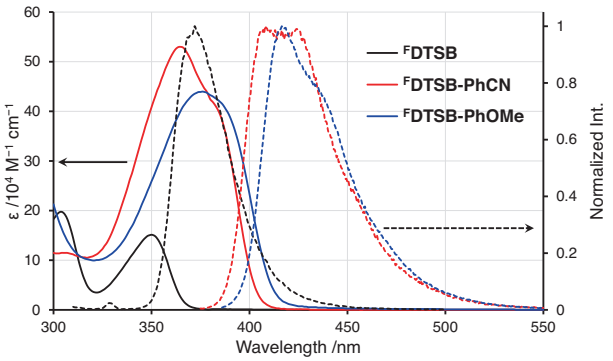

Fig. 3 UV-vis absorption (solid lines) and fluorescence spectra (dashed lines) of ^{F}DTSB compounds in toluene

Table 1 Optical data of ^{F}DTSB compounds

Compound	λ_{max}(abs)[a]/nm	λ_{max}(fl)[b]/nm	Φ_{fl}[c]/%	λ_{max}(phos)[d]/nm
^{F}DTSB	304, 350	372	<0.02	449
^{F}DTSB-PhCN	365	408	0.07	530
^{F}DTSB-PhOMe	376	417	0.12	529

[a]Absorption maxima in toluene at r.t.

[b]Fluorescence maxima in toluene at r.t.

[c]Absolute fluorescence quantum yield in toluene at r.t.

[d]Phosphorescence maxima in the 2-MeTMF glass matrix at 77 K

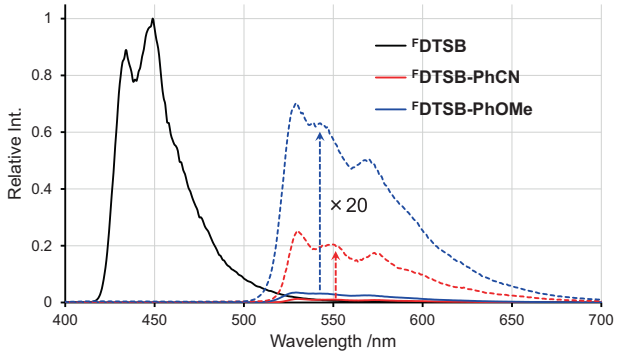

Fig. 4 Phosphorescence spectra of thiaborin compounds in the 2-MeTHF glass matrix at 77 K

the charge-separated excited states and offers evidence of the presence of the D − A intramolecular interaction in **^{F}DTSB-PhOMe**, in which the **^{F}DTSB** unit works as an acceptor, as we have expected. The fluorescence quantum yield (QY) of **^{F}DTSB** was so weak that it could not be determined (Table 1). The QYs of **^{F}DTSB-PhCN** and **^{F}DTSB-PhOMe** were 7% and 12% in toluene, respectively, indicating a slight improvement from that of **^{F}DTSB**. Next, phosphorescence spectra were measured in 2-MeTHF (Fig. 4). In agreement with the phosphorescence properties of small triarylborane molecules [31–34], **^{F}DTSB** showed bright greenish phosphorescence at 77 K. This indicates the fast intersystem crossing (ISC) of **^{F}DTSB**, which likely decreased the fluorescence QY at room temperature. **^{F}DTSB-PhCN** and **^{F}DTSB-PhOMe** also exhibited phosphorescence with maxima at 530 and 529 nm, respectively. Their phosphorescence intensities were much lower than that of **^{F}DTSB**, indicating the slower ISC for **^{F}DTSB-PhCN** and **^{F}DTSB-PhOMe** that resulted in the improvement of the fluorescence QYs.

Preparation of ^{F}DTSB polymers

The extended conjugation of cross-coupled compounds **^{F}DTSB-PhCN** and **^{F}DTSB-PhOMe** motivated us to synthesize conjugated polymers composed of **^{F}DTSB**. As comonomers, electron-rich bithiophene and dithienosilole units were employed to form D − A-type polymers. The

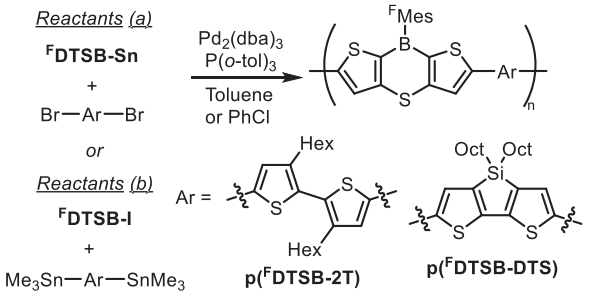

Scheme 2 Synthesis of ^{F}DTSB-based p−π* conjugated polymers

Table 2 Molecular weights of ^{F}DTSB-based p−π* polymers

Polymer	Reactants	M_n	M_w/M_n
p(^{F}DTSB-2T)	(a)	15,000	1.97
p(^{F}DTSB-2T)	(b)	9200	2.43
p(^{F}DTSB-DTS)	(a)	9000	1.76
p(^{F}DTSB-DTS)	(b)	6400	2.16

Stille cross-coupling reactions were carried out for **^{F}DTSB-Sn** or **^{F}DTSB-I** and aryl dibromide or ditin, respectively (Scheme 2). Chlorobenzene and toluene were used as the reaction solvents for the preparation of **p(^{F}DTSB-2T)** and **p(^{F}DTSB-DTS)**, respectively. The obtained polymers were purified by reprecipitation, and the molecular weights were determined by GPC in THF using polystyrene standards (Table 2). The obtained polymers **p(^{F}DTSB-2T)** showed nearly identical ^{1}H NMR spectra regardless of the different combinations of the reactants (a and b in Scheme 2, Fig. S4). For **p(^{F}DTSB-2T)**, we used the polymer synthesized from reactants (a) in the following photophysical investigations because it has a higher molecular weight than **p(^{F}DTSB-2T)** prepared from reactants (b). Similarly, the molecular weight of **p(^{F}DTSB-DTS)** prepared from reactants (a) was also higher than that of **p(^{F}DTSB-DTS)** prepared from reactants (b). However, as unidentified peaks were detected in the ^{1}H NMR spectrum for **p(^{F}DTSB-DTS)** prepared from reactants (a) (Fig. S4), we chose the polymer prepared from reactants (b) for the following investigations. The molecular weights of **p(^{F}DTSB-DTS)** were lower than those of **p(^{F}DTSB-2T)**, possibly due in part to the use of toluene as the reaction solvent in the preparation of **p(^{F}DTSB-DTS)**, as most of the obtained polymers were insoluble when chlorobenzene was used as the reaction solvent. The solubility of **p(^{F}DTSB-2T)** in organic solvents was relatively low; it was soluble in THF and chloroform but hardly soluble in toluene and dichloromethane. On the other hand, **p(^{F}DTSB-DTS)** was soluble not only in THF and chloroform but also in toluene, indicating that the solubility of **p(^{F}DTSB-DTS)** is slightly higher than that of **p(^{F}DTSB-2T)**. All the polymers were sufficiently stable in air, as in the case of the monomers, and did not decompose even after storage in air at room temperature for one year.

To confirm the thermal stability of the polymers, thermogravimetric analysis (TGA) was performed in air (Fig. S5). The 5% weight loss temperatures (T_d^5) of **p(FDTSB-2T)** and **p(FDTSB-DTS)** were 328 °C and 266 °C, respectively. TGA was also acquired for poly(3-hexyl)thiophene (**P3HT**) as a comparison to reveal $T_d^5 = 409$ °C. This indicates that the thermal stability of the p-π*-conjugated thiaborin polymers was lower than that of fully conjugated polythiophene. However, the TGA profiles of **p(FDTSB-2T)** and **p(FDTSB-DTS)** suggest no decomposition of the thiaborin polymers up to approximately 150 °C, indicating sufficient stability for usual handling. No melting/glass transition was detected in the differential scanning calorimetry (DSC).

Optical properties of FDTSB polymers

The absorption maximum of **p(FDTSB-2T)** was redshifted by 83 nm from that of **FDTSB** in toluene, again demonstrating the effective extension of the conjugation (Fig. 5, Table 3). Interestingly, the solubility of **p(FDTSB-2T)** in common organic solvents was so low that the absorption spectra were different before and after filtration of the solution through a membrane filter (Fig. S6). Before filtration, absorption bands appeared in the range of 500 to 600 nm, suggesting the formation of small aggregates. The appearance of the band at long wavelengths is noteworthy because it indicates that **p(FDTSB-2T)** has strong intermolecular interactions despite the presence of the bulky FMes group. Indeed, the spin-coated film exhibited a strong absorption in the same region as the new band, again corroborating the strong intermolecular interactions of **p(FDTSB-2T)** in the solid state (Fig. 5). This tendency is inconsistent with the weak intermolecular interactions in the single-crystal structure of **FDTSB-PhOMe**. The strong intermolecular interactions of **p(FDTSB-2T)** may be induced by the 1D polymeric conjugated structure. The absorption band of **p(FDTSB-DTS)** was shifted to longer wavelengths relative to that of **p(FDTSB-2T)**, which is likely due to the higher planarity and the stronger electron-donating property of DTS than the bithiophene unit. As the molecular weight of **p(FDTSB-DTS)** prepared from reactants (b) is relatively low ($M_n = 6400$), the absorption spectra were compared with those prepared from reactants (a) (Fig. S7). Despite the higher molecular weight of **p(FDTSB-DTS)** prepared from reactants (a) ($M_n = 9000$), the absorption edges were nearly the same for the two polymers obtained from the different monomer combinations. This indicated that **p(FDTSB-DTS)** prepared from reactants (b) nearly reached the effective conjugation length regardless of the low molecular weight. Compared with **p(FBDT-DTS)** [16], the absorption maximum of **p(FDTSB-DTS)** was blueshifted by 33 nm in toluene. This may be due to the weaker electron-withdrawing property of the FDTSB unit than the FBDT unit, resulting in the weaker D − A interaction. Different from **p(FDTSB-2T)**, the absorption maxima of **p(FDTSB-DTS)** in solution and the film state were nearly the same. However, new shoulder peaks appeared at longer wavelengths, suggesting the presence of weak intermolecular interactions. The small degree of the redshift in **p(FDTSB-DTS)** is likely due to the octyl groups on the silicon atom located perpendicular to the π-plane of DTS. On the other hand, as reported previously, the absorption spectra of **p(FBDT-DTS)** in solution and the film state were almost identical [16], showing no intermolecular interactions at all. Therefore, the redshift of **p(FDTSB-DTS)** in the film state clearly indicates that the introduction of the thiaborin structure enhances the intermolecular interactions. XRD measurements were also performed for the borepin polymers to investigate the intermolecular interactions; however, no obvious peaks were detected (Fig. S8). This indicates the low crystallinity of the polymers. All solvents examined, including Lewis basic pyridine, had no effect on the absorption spectra of either of the polymers (Fig. S9 and S10, and Table S2). This indicates that the Lewis acidity of **FDTSB** and its polymers are weak, similar to those of **FBDT** and **p(FBDT-DTS)**, likely due to the steric hindrance of FMes groups [16].

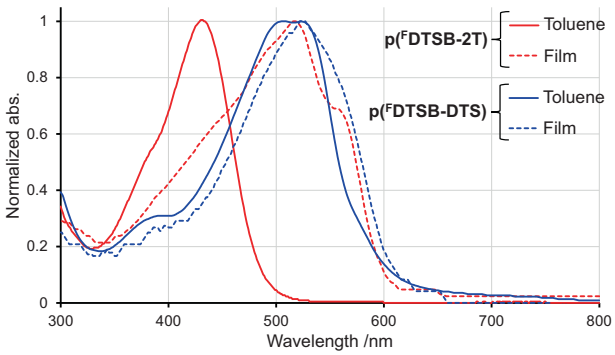

Fig. 5 UV-vis absorption spectra of FDTSB-based p−π* conjugated polymers

As noted in the absorption bands, the fluorescence bands of **p(FDTSB-DTS)** appeared in the longer wavelength region compared with those of **p(FDTSB-2T)** (Fig. 6). In the spectrum of **p(FDTSB-DTS)**, clear vibronic structures were observed, reflecting the highly rigid structure of DTS. The fluorescence QYs of the polymers were higher than that of **FDTSB** in toluene (Table 3). In particular, the QY of **p(FDTSB-DTS)** was moderately high at 33% and comparable to that of **p(FBDT-DTS)** [16]. In contrast to the clear solvatochromic behavior of **p(FBDT-DTS)** in the fluorescence spectra, solvent polarity had a minimal influence on the fluorescence spectra of thiaborin polymers **p(FDTSB-2T)** and **p(FDTSB-DTS)** (Figs. S11 and S12). This again demonstrates the weaker electron-withdrawing property of

Table 3 Optical and electrochemical data of ^{F}DTSB-based p−π* conjugated polymers

Compound	λ_{max}(abs)[ab]/nm	λ_{max}(fl)[bc]/nm	Φ_{fl}[d]/%	E_g[e]/eV	V_{ox}[f]/V	V_{red}[g]/V
p(^{F}DTSB-2T)	433 (521)	532 (669)	0.19	2.56	0.66	-[h]
p(^{F}DTSB-DTS)	525 (530)	563 (686)	0.33	2.03	0.61	−1.78

[a]Absorption maxima in toluene at r.t.

[b]Values in parentheses are for the spin-coated film

[c]Fluorescence maxima in toluene at r.t.

[d]Absolute fluorescence quantum yield in toluene at r.t.

[e]Band gap estimated from the onset absorption in toluene

[f]Onset of the oxidation wave of the deposited film in CV using 0.1 M tetrabutylammonium hexafluorophosphate in MeCN as the supporting electrolyte and a scan rate of 50 mV s^{-1}

[g]Onset of the reduction wave of the deposited film in CV

[h]Not observed

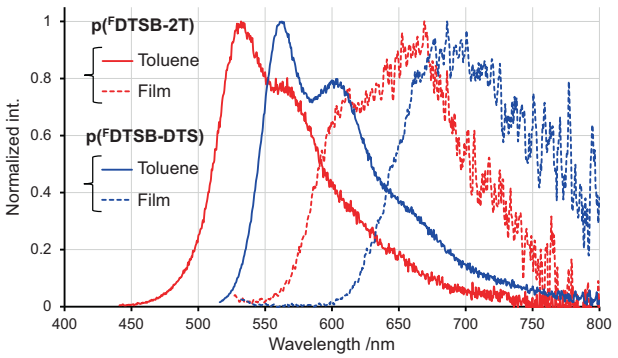

Fig. 6 Fluorescence spectra of ^{F}DTSB-based p−π* conjugated polymers

the ^{F}DTSB unit than the ^{F}BDT unit. The fluorescence bands obtained in the film state were redshifted from those in solution, as was observed in the absorption spectra.

Computational study

Next, time-dependent density functional theory (TD-DFT) calculations were performed on a Gaussian 16 program to investigate the electronic structures of thiaborin polymers (Fig. 7). Model oligomers **o(^{F}DTSB-2T)** and **o(^{F}DTSB-DTS)** were optimized at the B3LYP/6-31 G(d) level of theory. The optimized geometry of **o(^{F}DTSB-DTS)** was almost planar, whereas that of **o(^{F}DTSB-2T)** deviated from planarity at the bithiophene units (Fig. S13). The calculated $S_0 \rightarrow S_1$ transition was HOMO → LUMO transition for all the oligomers. The lowest transition energy of **o(^{F}DTSB-DTS)** was smaller than that of **o(^{F}DTSB-2T)**, reflecting the high planarity of DTS. For both oligomers, an evident contribution of the p-orbital on boron was seen in the LUMOs, indicating the effective p−π* interaction as observed in other p−π* conjugated materials. To confirm the effect of the bridging of the thiophene rings with sulfur atoms, the ^{F}BDT model oligomer **o(^{F}BDT-DTS)** was also calculated. The dihedral angles between the two thiophene rings were 0.6° for the ^{F}DTSB unit in **o(^{F}DTSB-DTS)**, whereas they were approximately 37° for the ^{F}BDT unit in **o(^{F}BDT-DTS)**. The lowest transition energy of **o(^{F}BDT-DTS)** was smaller than that of **o(^{F}DTSB-DTS)**, in agreement with the experimental results (Table 3). Interestingly, the LUMO energy levels of **o(^{F}DTSB-DTS)** and **o(^{F}BDT-DTS)** were almost the same, whereas the HOMO energy level of **o(^{F}DTSB-DTS)** was much lower than that of **o(^{F}BDT-DTS)**. This means that the HOMO of **o(^{F}DTSB-DTS)** was greatly stabilized by the high aromaticity of the thiaborin structure. On the other hand, the LUMO of **o(^{F}DTSB-DTS)** would be destabilized by the aromaticity of the thiaborin structure but might be neutralized by the effective p−π* interaction and the high planarity. The aromaticity of the ^{F}DTSB structure was confirmed from the nucleus-independent chemical shift (NICS) values. The calculated NICS(1) value for **^{F}DTSB** was −4.85 (Table S1), which again demonstrated the moderately high aromaticity of the thiaborin structure in the ^{F}DTSB unit.

Electrochemical properties

Finally, we performed cyclic voltammetry (CV) experiments on the present polymer films in acetonitrile containing tetrabutylammonium hexafluorophosphate as the supporting electrolyte. In the cathodic voltammogram, **p(^{F}DTSB-DTS)** showed a reduction peak with onset at −1.78 V (Fig. 8, Table 3). The estimated LUMO energy level of **p(^{F}DTSB-DTS)** was −3.02 eV, almost the same as that of **p(^{F}BDT-DTS)** [16] and consistent with the calculation results (*vide supra*). No cathodic peaks were observed for **p(^{F}BDT-2T)**. In the anodic voltammograms, both polymers exhibited broad oxidation peaks (Fig. 8). The CV curves were irreversible, which may be partly because the films were used for the measurements. The films were decomposed and partially peeled off from the electrode after the measurements. Two small anodic peaks at approximately 0.7 V were observed in the cyclic voltammograms of **p(^{F}DTSB-2T)**. To confirm that these small peaks were not ghost peaks, CV was also performed on **p(^{F}DTSB-2T)** prepared from reactants (b). Although the

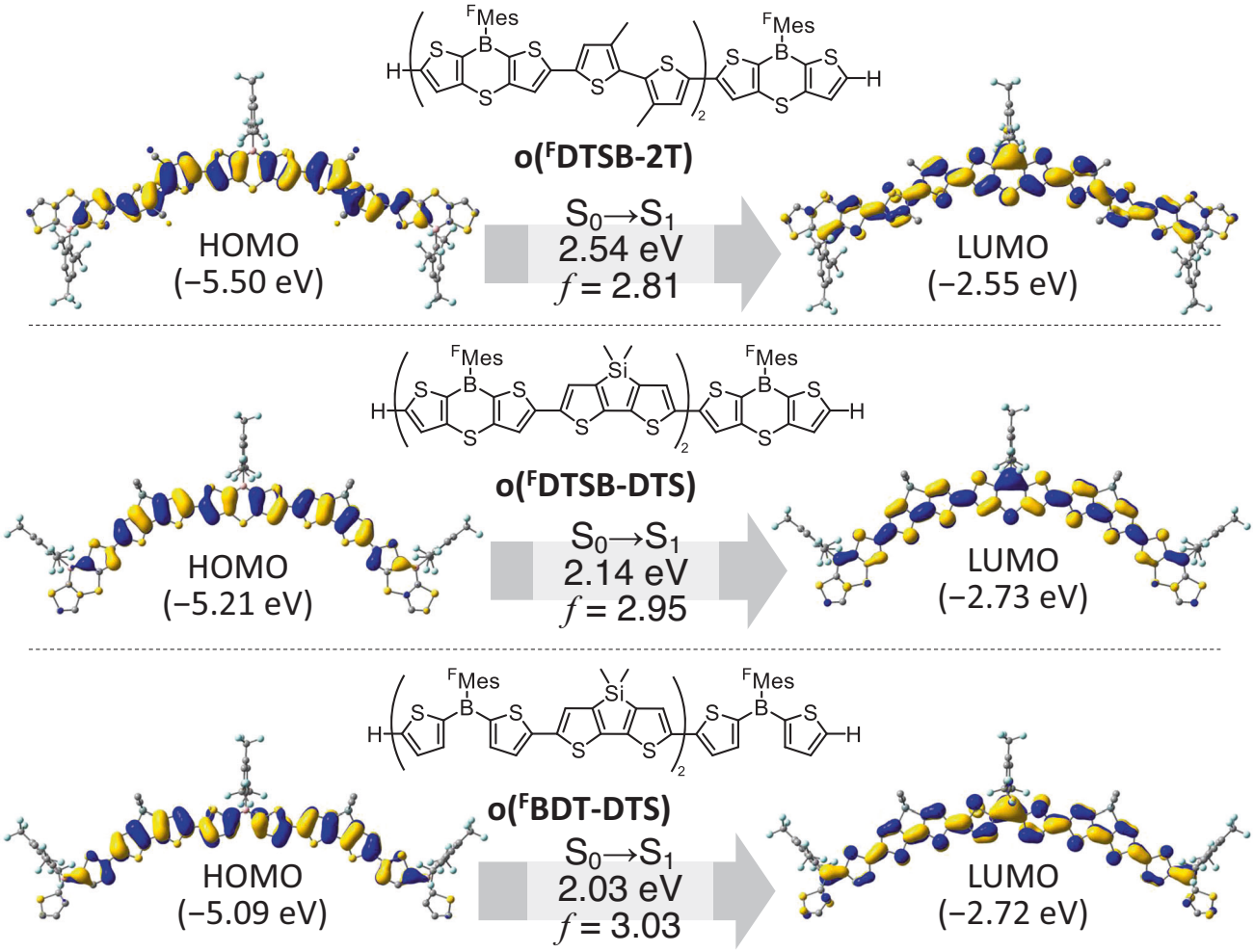

Fig. 7 Calculated molecular orbitals of **o(FDTSB-2T)**, **o(FDTSB-DTS)**, and **o(FBDT-DTS)** and their excitation energies, wavelengths, and oscillator strengths of allowed transitions obtained from TD-DFT calculations at the B3LYP/6-31 G(d) level of theory

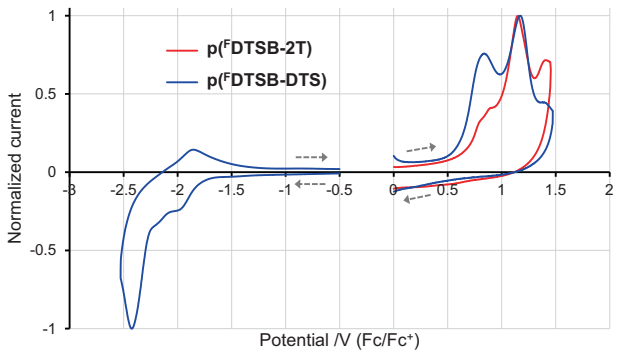

Fig. 8 Cyclic voltammograms of **p(FDTSB-2T)** and **p(FDTSB-DTS)** films in acetonitrile with 0.1 M $TBAPF_6$ at a scan rate of 50 mV/s

peaks were not separated, a weak anodic peak was detected in **p(FDTSB-2T)** prepared from reactants (b) at a similar potential as in the polymer prepared from (a), supporting that the anodic peaks at approximately 0.7 V originate from the oxidation of the polymer structure (Fig. S14). The HOMO energy levels estimated from the anodic signals were −5.46 eV and −5.41 eV for **p(FDTSB-2T)** and **p(FDTSB-DTS)**, respectively. The energy difference of the HOMO between **p(FDTSB-2T)** and **p(FDTSB-DTS)** was only 0.05 eV despite the much larger transition energy of **p(FDTSB-2T)** than that of **p(FDTSB-DTS)** in solution (Table 3). This clearly demonstrated that the strong intermolecular interactions of **p(FDTSB-2T)** raised the HOMO energy level, diminishing the HOMO – LUMO energy gap of **p(FDTSB-2T)** in the solid state.

Conclusion

We have synthesized p−π* conjugated polymers composed of FMes-substituted thiaborin building blocks. The monomeric thiaborin compounds showed weak fluorescence at room temperature and strong phosphorescence at 77 K. We have prepared the first examples of thiaborin-based p−π* conjugated polymers. Different from conventional p−π* conjugated systems, thiaborin-based p−π* conjugated polymers

exhibit strong intermolecular interactions in the solid state, attesting to their potential applications as semiconductors for optoelectronic devices.

Funding This work was supported by JSPS KAKENHI Grant Numbers JP19K15543 and JP22K14666.

Compliance with ethical standards

Conflict of interest The authors declare no competing interests.

References

1. Facchetti A. π-Conjugated polymers for organic electronics and photovoltaic cell applications. Chem Mater. 2011;23:733–58.
2. Ostroverkhova O. Organic optoelectronic materials: mechanisms and applications. Chem Rev. 2016;116:13279–412.
3. Inal S, Rivnay J, Suiu A-O, Malliaras GG, McCulloch I. Conjugated polymers in bioelectronics. Acc Chem Res. 2018;51:1368–76.
4. Fratini S, Nikolka M, Salleo A, Schweicher G, Sirringhaus H. Charge transport in high-mobility conjugated polymers and molecular semiconductors. Nat Mater. 2020;19:491–502.
5. Ren Y, Jäkle F. Merging thiophene with boron: new building blocks for conjugated materials. Dalton Trans. 2016;45:13996–4007.
6. Ji L, Griesbeck S, Marder TB. Recent developments in and perspectives on three-coordinate boron materials: a bright future. Chem Sci. 2017;8:846–63.
7. Helten H. Doping the backbone of π-conjugated polymers with tricoordinate boron: synthetic strategies and emerging applications. Chem Asian J. 2019;14:919–35.
8. Yin X, Liu J, Jäkle F. Electron-deficient conjugated materials via p–π* conjugation with boron: extending monomers to oligomers, macrocycles, and polymers. Chem Eur J. 2021;27:2973–86.
9. Hudnall TW, Chiu C-W, Gabbaï FP. Fluoride ion recognition by chelating and cationic boranes. Acc Chem Res. 2009;42:388–97.
10. Wade CR, Broomsgrove AEJ, Aldridge S, Gabbaï FP. Fluoride ion complexation and sensing using organoboron compounds. Chem Rev. 2010;110:3958–84.
11. Mellerup SK, Wang S. Boron-based stimuli responsive materials. Chem Soc Rev. 2019;48:3537–49.
12. Matsumi N, Naka K, Chujo Y. Extension of π-conjugation length via the vacant p-orbital of the boron atom. Synthesis of novel electron deficient π-conjugated systems by hydroboration polymerization and their blue light emission. J Am Chem Soc. 1998;120:5112–3.
13. Matsumi N, Naka K, Chujo Y. Poly(*p*-phenylene-borane)s. Novel organoboron π-conjugated polymers via grignard reagent. J Am Chem Soc. 1998;120:10776–7.
14. Yin X, Chen J, Lalancette RA, Marder TB, Jäkle F. Highly electron-deficient and air-stable conjugated thienylboranes. Angew Chem Int Ed. 2014;53:9761–5.
15. Yin X, Guo F, Lalancette RA, Jäkle F. Luminescent main-chain organoborane polymers: highly robust, electron-deficient poly(-oligothiophene borane)s via stille coupling polymerization. Macromolecules. 2016;49:537–46.
16. Adachi Y, Ooyama Y, Ren Y, Yin X, Jäkle F, Ohshita J. Hybrid conjugated polymers with alternating dithienosilole or dithienogermole and tricoordinate boron units. Polym Chem. 2018;9:291–9.
17. Adachi Y, Nabeya T, Kawakami K, Yamaji K, Jäkle F, Ohshita J. Optical characteristics of hybrid macrocycles with dithienogermole and tricoordinate boron units. Chem Eur J. 2021;27:3306–14.
18. Adachi Y, Kondo K, Yin X, Jäkle F, Ohshita J. *m*-Phenylene linked macrocycle composed of electron-rich dithienogermole and electron-deficient tricoordinate boron units. Polymer 2022;239:124404.
19. Meng B, Ren Y, Liu J, Jäkle F, Wang L. p–π conjugated polymers based on stable triarylborane with n-type behavior in optoelectronic devices. Angew Chem Int Ed. 2018;57:2183–7.
20. Welsh TA, Laventure A, Alahmadi AF, Zhang G, Baumgartner T, Zou Y, et al. Borane incorporation in a non-fullerene acceptor to tune steric and electronic properties and improve organic solar cell performance. ACS Appl Energy Mater. 2019;2:1229–40.
21. Yu Y, Dong C, Alahmadi AF, Meng B, Liu J, Jäkle F, et al. A p-π* conjugated triarylborane as an alcohol-processable n-type semiconductor for organic optoelectronic devices. J Mater Chem C. 2019;7:7427–32.
22. Adachi Y, Nomura T, Tazuhara S, Naito H, Ohshita J. Thiophene-based twisted bistricyclic aromatic ene with tricoordinate boron: a new n-type semiconductor. Chem Commun. 2021;57:1316–9.
23. Mitsudo K, Shigemori K, Mandai H, Wakamiya A, Suga S. Synthesis and properties of dithieno-fused 1,4-azaborine derivatives. Org Lett. 2018;20:7336–40.
24. Yan Y, Sun Z, Li C, Zhang J, Lv L, Liu X, et al. Thiophene-fused 1,4-thiaborins: synthesis, structures and properties. Asian J Org Chem. 2017;6:496–502.
25. Chiu C-Y, Kim B, Gorodetsky AA, Sattler W, Wei S, Sattler A, et al. Shape-shifting in contorted dibenzotetrathienocoronenes. Chem Sci. 2011;2:1480–6.
26. Wang X-Y, Jiang W, Chen T, Yan H-J, Wang Z-H, Wan L-J, et al. Molecular evidence for the intermolecular S···S interaction in the surface molecular packing motifs of a fused thiophene derivative. Chem Commun. 2013;49:1829–31.
27. Antonijević IS, Janjić GV, Milčić MK, Zarić SD. Preferred geometries and energies of sulfur–sulfur interactions in crystal structures. Cryst Growth Des. 2016;16:632–9.
28. Higashino T, Ishida K, Sakurai T, Seki S, Konishi T, Kamada K, et al. Pluripotent features of doubly thiophene-fused benzodiphospholes as organic functional materials. Chem Eur J. 2019;25:6425–38.
29. Kruszewski J, Krygowski TM. Definition of aromaticity basing on the harmonic oscillator model. Tetrahedron Lett. 1972;13:3839–42.
30. Krygowski TM, Szatylowicz H, Stasyuk OA, Dominikowska J, Palusiak M. Aromaticity from the viewpoint of molecular geometry: application to planar systems. Chem Rev. 2014;114:6383–422.
31. Ma J-L, Liu H, Li S-Y, Li Z-Y, Zhang H-Y, Wang Y, et al. Metal-free room-temperature phosphorescence from amorphous triarylborane-based biphenyl. Organometallics. 2020;39:4153–8.
32. Wu Z, Nitsch J, Schuster J, Friedrich A, Edkins K, Loebnitz M, et al. Persistent room temperature phosphorescence from triarylboranes: a combined experimental and theoretical study. Angew Chem Int Ed. 2020;59:17137–44.
33. Adachi Y, Yamada K, Ohshita J. Synthesis and optical properties of anthryl-substituted tetracyclic borepins. Chem Lett. 2022;51:654–7.
34. Adachi Y, Arai F, Yamada K, Kurihara M, Ohshita J. Optical properties of boron-incorporated analogues of tetrathienoanthracene. Organometallics. 2022;41:1225–31.

Publisher's note Springer Nature remains neutral with regard to jurisdictional claims in published maps and institutional affiliations.

Springer Nature or its licensor (e.g. a society or other partner) holds exclusive rights to this article under a publishing agreement with the author(s) or other rightsholder(s); author self-archiving of the accepted manuscript version of this article is solely governed by the terms of such publishing agreement and applicable law.